Alessandro Corsini[(1)] and Marco Mulas[(1*)]

[(1)] Department of Chemical and Geological Sciences, University of Modena and Reggio Emilia
Via G. Campi 103, 41125 Modena, Italy

[(*)] corresponding author: e-mail: marco.mulas@unimore.it. Tel: +39-059-2058498. Fax: +39-059-2055887

Use of ROC curves for early warning of landslide displacement rates in response to precipitation (Piagneto landslide, Northern Apennines, Italy)

Abstract

Active landslides are generally characterized by variations in displacement rate in response to cumulated precipitation. Velocities that are only exceeded in a limited number of days during the year, might be considered as critical events, since they might determine, or prelude to, a significant evolution of the landslide. The purpose of this paper is to present a novel approach based on the use of ROC curves (Receiver Operating Characteristic curves) for assessing cumulated precipitation thresholds that can provide early warning for the occurrence of critical events such as the exceedance of rare displacement rates. The approach has been developed and tested in the Piagneto landslide, an active complex rock slide – debris slide in the Northern Apennines of Italy, for which a 5 years continuous surveying monitoring dataset is available. On the basis of the first 4 years of monitoring data (training dataset), threshold curves relating cumulative precipitation (mm) to precipitation moving windows (days) have been generated by using different benchmarks that, in literature, are used to estimate the maximum predictive performance of ROC curves. These threshold curves have been successfully validated using the last 1 years of monitoring data (validation dataset). They have then been used to simulate how they might help defining different early warning levels in due advance. The proposed methodology can be replicated in any landslide for which a monitoring dataset that includes recurrent acceleration events in response to precipitation is available.

Keywords

ROC curves, Landslides, Displacement rate, Cumulated precipitation, Early warning, Northern Apennines

Introduction

Active landslides are generally characterized by variations in displacement rate in response to cumulated rainfall. Velocities that are only exceeded in a limited number of days during the years, might be considered as critical events, since they might determine, or prelude to, a significant evolution of the landslide.

The analysis and prediction of changes in landslide displacement rates in response to rainfall can support the assessment of early warning rules. Approaches that can be used to predict displacement rates can be classified into three main categories (Li et al. 2012): deterministic physical models, nonlinear models and statistics models. Physical models are based upon deterministic laws linking changes of groundwater pressure induced by rainfall to changes of the safety factor and, consequently, changes in displacement rate. Laws exist for a rigid-perfectly plastic slope behaviour (Iverson 2000) as well as for a viscous behaviour (Vulliet and Hutter 1988; Bracegirdle et al. 1991; Butterfield 2000; Leroueil 2000). Physical models can also make use of numerical codes that couple groundwater recharge models to slope stability models in order to deterministically forecast displacement rates (Corominas et al. 2005; Herrera et al. 2009; Belle et al. 2014; Bernardie et al. 2014; Abellán et al. 2015; Bernardie et al. 2015; Schädler et al. 2015). Nonlinear models are based upon computational approaches that aim to represent the posterior distribution of displacement using functions based on training data and prior distribution. They make use of support vector machines, Gaussian process and other machine learning techniques (Zhang et al. 2006; Li et al. 2012; Li and Kong 2014; Liu et al. 2014) as well as artificial neural networks (Mayoraza and Vullietb 2002). Statistical models are based upon probabilistic relationships between rainfall and displacement data based on principal component analysis (Nordvik and Nyrnes 2009) or cross correlation techniques (Lollino et al. 2006).

The purpose of this paper is to present a novel approach based on the use of ROC curves (Receiver Operating Characteristic curves) for statistically assessing cumulated precipitation thresholds that can provide early warning for the occurrence of events represented by the exceedance of rare displacement rates. The ROC curves are binary discriminant classifiers that are widely used in many fields of science including geosciences (Donner and Barbosa 2008). In slope instability studies, their most common use is the analysis of the predictive performance and the validation of landslide susceptibility maps (Chung and Fabbri 2003). To the author's best knowledge, this versatile and simple statistical method has not yet been used for the analysis of long-term displacement monitoring data versus cumulated precipitation. The approach has been developed and tested in the Piagneto landslide, an active complex rock slide – debris slide in the Northern Apennines of Italy that has been monitored for more than five years (from 2009 to 2014) by means of a Robotic Total Station (RTS) (Corsini et al. 2015b). Over the same period, an hourly precipitation dataset is available from precipitation gauges located just a km away from the landslide. The results obtained by the application of the proposed method extend the findings of the conference abstract by Corsini et al (2015a) and now include threshold curves relating cumulative precipitation (mm) versus precipitation moving windows (days) that can be used, as the discussion exemplifies, for early warning purposes.

Case study and dataset

The Piagneto landslide is located in the Northern Apennines of Italy (Fig. 1a). It includes two main sub-units (Corsini et al. 2013a): a compound rock slide sub-unit to the northwest (G1) and a complex rock slide – debris slide sub-unit to the southeast (G2). This paper deals with sub-unit G2, that extends from 1050 to 800 m a.s.l. with a maximum length of 620 m, a width of 200 m and an affected area of 50000 m^2 (Fig. 1b). Average slope angle is around 22°, but due to the presence of gravitational scarps, trenches and counter slopes, this parameter varies from 50° to less than 10° along the landslide. Sub-unit G2 includes an upper rock slide sector (G2a) and a lower debris slide sector (G2b) (Fig. 1c). The rock slide G2a is constituted by large decametric disarranged blocks of limestone (GSBa, "Calcari Cavernosi" Formation of the Triassic) sliding over the underlying clay shales (AVC, "Argille Variegate con Calcari" Formation of the Cretaceous). Due to the lack of direct measurements, the depth and dip of the basal sliding surface are not precisely known. However, on the basis of local geologic and geomorphic conditions, Corsini et al. (2013b) have estimated the depth of the sliding surface to a maximum of 50 m with an inclination varying, due to transition from rotational to traslational movement, from sub-vertical in the upper part of the rockslide to approximately 20° in its lower part. The debris slide G2b is made of metric limestone debris deposited over clay shales (AVC) and sandstone flysch (CEV, Arenarie di Cervarola Formation of the Oligocene-Miocene) (Fig. 1b). In September 1972, a major reactivation of the debris slide buried a stretch of 150 m of National Road (Moratti and Pellegrini, 1977). Such paroxysmal event was triggered by the collapse of the frontal portion of the rock slide after severe precipitation conditions.

The landslide displacement dataset includes 5 years of monitoring data obtained with a RTS surveying 20 prisms located in the unstable slope as well as reference prisms in stable areas (Corsini et al. 2015b). Prisms were surveyed with the polar method and at duty cycles of 2 hours. Prisms with identifier from G2_01 to G2_08 were measured from 08/11/2009

to 12/12/2014 while prisms from G2_09 to G2_20 were measured from 25/07/2010 to 12/12/2014 (fig. 2b). The irregular spatial distribution of monitoring prisms in the slope, which does not cover each landslide element, is due to practical constrains caused by the dense vegetation in the slope. The RTS is located exactly opposite to the landslide slope, at a distance of slightly more than 1 km and at approximately the same elevation of monitoring prisms, so the line of sight of the RTS is almost equivalent to the downslope azimuth of slope movements (Corsini et al. 2013b). Since the vertical component of displacements has proven negligible compared to the planar one, the variation in time of the slope distance between RTS and prisms can be considered as a significant measure of landslide displacement. This allows avoiding using polar coordinates, which being derived by the combination of angular and distance measures are generally affected by a lower precision than the inclined distance alone.

Generally, deep-seated rock slides are characterised by complex subsoil water circulation that hardly allows to directly link precipitation input to unsteady phases of a mass movement (Ronchetti et al. 2007). However, in the Piagneto monitoring dataset, a direct correlation between precipitation and movement rates is quite evident by data itself, especially in the lower part of the rock slide and in the debris slide area (Fig. 2a). Total recorded displacements over the 5 years of monitoring vary from about 10 to 80 cm and movement rates increase from autumn to spring (wet season) as well as after specific precipitation events. Thus, it makes sense to seek for a link between precipitation and phases of higher movement rates.

For the aim of this research, the monitoring dataset has been divided into a training dataset (4 years from 08/11/2010 to 04/11/2013) and a validation dataset (1 year from 04/11/2013 to 12/12/2014) (Fig. 2a). At the same time, the lower part of the rock slide has been subdivided into “front”, “middle” and “rear” units (Fig. 2b). In the training dataset, monitoring prisms in the lower part of the rock slide show an average velocity ranging from 65 to 188 mm/year, with prisms in the “front” units generally move faster than prisms in “middle” and “rear” units. Prisms in the debris slide, on the other hand, show an average velocity ranging from 37 to 80 mm/year (Fig. 2c). The analysis of the frequency distribution of velocity in the training dataset allows the velocity values with a 5% exceedance probability to be determined for each prism (hereafter referred to as $V_{95\%}$). The $V_{95\%}$ varies from 150 to 430 mm/year in the different rock slide units (Fig. 2d). In general, the $V_{95\%}$ in the “front” units is in the order of 300 to 400 mm/year. This value is significantly higher than the $V_{95\%}$ in the “middle” and “rear” units, that is on average 223 mm/year. The $V_{95\%}$ of prisms in the debris slide are even lower, below 200 mm/year.

The precipitation dataset covers the same time interval of the displacement dataset. It has been obtained from the Collagna rain gauge, which is part of the institutional regional meteorological monitoring network managed by ARPAE Emilia-Romagna. This precipitation gauge is located at only 940 m distance from the landslide site at an elevation of 832 m a.s.l. similar to that of landslide site. Thus, it is considered representative of the precipitation at the landslide site. By using a heated precipitation-gauge, it includes indistinctly the hourly and daily precipitation caused by rainfall and snowfall. For the scope of this research the delayed contribute introduced by snow melting has not been taken in consideration, thus it could bias the accuracy of the final result.

Methodology

The ROC Curve (Receiver Operating Characteristic) is a commonly used technique to display the results of a binary classification between the outcomes of a predictive model (or classifier) and the actual occurrence of the forecasted event (Donner and Barbosa 2008). In simple terms, if a model predicts a positive value of a given variable (event forecast) and the value of the variable is actually positive (event), a True Positive (TP) prediction is obtained. At the opposite, if the value of the variable is actually negative (no event), a False Positive (FP) prediction is obtained. True Negative (TN) and False Negative (FN) predictions are classified following similar logical combinations and, from all these scores, the True Positive Rate (TP-Rate) and False Positive Rate (FP-Rate) can be determined (see Fig. 3 for formulations). The ideal classifier should return a TP-rate of 1 and a FP-rate of 0, meaning it predicted all the events with no false alarm. The ROC curves are plots of the TP-Rate versus the FP-Rate which are obtained by considering different values of the model output to forecast the event.

In this research, ROC curves have been applied to the Piagneto landslide monitoring dataset in order to quantitatively estimate the relationship between the occurrence of displacement velocities above a given threshold value (event) and the antecedent precipitation, cumulated over different time windows (event forecast). The approach is exemplified in figure 3a, where a 350 mm/year velocity and a 150 mm precipitation arbitrary thresholds are set. If, in a given day, the cumulated precipitation reaches a certain value (event forecast) and the velocity of the monitoring prism is actually exceeding the predefined threshold (event), then a TP is obtained. On the other hand, a FP is obtained if the cumulated precipitation reaches the same value (event forecast), but the velocity of the prism remains below the predefined threshold (no event). In similar way, TN and FN events are also defined. A full ROC curve can thus be obtained, for a given velocity threshold

and a specific time window of cumulated precipitation, by plotting the TP-rate and FP-rate associated to the various value of cumulated precipitation recorded in each day of the dataset (Fig. 3c). In practice, by keeping a fixed velocity threshold and a given cumulated time window, any value of recorded cumulated precipitation is considered as a possible event forecast. A number of different ROC curves can then be obtained by changing the duration of the time window of cumulated precipitation.

The discriminant capacity of a model prediction can be assessed on the basis of the area under the ROC curve (AUC), included in the range 0 to 1 (Swets, 1988). Models that return an AUC higher than 0.7 are generally considered to have an acceptable discriminant capacity (Hosmer and Lemeshow, 2000). In our approach, ROC curves with the higher AUC will indicate the duration of the precipitation moving window that provides the best discriminant capacity for predicting the event, i.e. the exceedance of the velocity threshold. Moreover, the specific predictive performance of each point constituting the ROC curve can be assessed on the basis of different benchmarks. One benchmark is the ratio between TP-rate and FP-rate, that can be represented by the orthogonal distance from the diagonal line of the diagram (so called "line of no discrimination", representing a random statistical distribution). The point at maximum distance (Max. Dist.) corresponds to a value of the predictive model (in our case, cumulated precipitation) that provides the maximum ratio between hits and false alarms (fig. 3c). Another possible benchmark is the Threat Score Index, i.e. the ratio between TP and the sum between TP, FP and FN (see Fig. 3b for formulation). The point with maximum TSI (Max. TSI), is the point corresponding to a value of the predictive model (in our case, cumulated precipitation) that provides the maximum ratio between hits and the sum of hits, false alarms and misses. Finally, in a ROC curve, the maximum value of the predictive model that is associated to a TP event can also be retrieved. In our method, it corresponds to the maximum precipitation (Max. TP-precipitation) associated to a TP event in the ROC curve. The methodology has been based on scripts in R environment (R Development Core Team, 2008) to perform the following processing steps.

- Separation of the monitoring dataset into a training dataset (4 years from 08/11/2009 to 04/11/2013) and a validation dataset (1 year from 04/11/2013 to 12/12/2014).
- Filtering of outliers from cumulative displacement time-series and down-sampling of the dataset to a 1-day-time interval. In practice, filtering was necessary in order to eliminate outliers caused by rare instrumental anomalies or incomplete atmospheric correction of RTS measurements. Filtering was based on calculation of the daily average value and the 7 days moving average value so to obtain a trend line and then, day by day, comparing the daily average with the 7 days average trend line and removing daily values that outlie from trend line for more than 0.5 sigma. In these cases, the removed daily value is replaced by the value of the trend line in that day. It should be stressed that the number of outliers was generally limited to 1 or 2 per week, thus the filtering did not alter the time series. On the other hand, not filtering outliers would have produced artefacts in the velocity time series.
- Analysis of velocity frequency distribution. In order to account for the fact each prism in the dataset is characterized by different displacement rates, we have considered as "event" the exceedance of $V_{95\%}$ velocity of the prism, i.e. the occurrence of displacement rates with a 5% exceedance probability in the dataset. The frequency distribution analysis thus returns the $V_{95\%}$ of each prism.
- Generation, with reference to each prism and to its specific $V_{95\%}$, of ROC curves related to time-window of cumulated precipitation of 1, 3, 5, 7, 10, 15, 20, 25, 30, 35, 40, 45, 50, 60, 70, 80, 90, 100, 110, 120 days. These curves are then displayed into a synoptic plot (Fig. 4a).
- Calculation of AUC of each ROC curve and generation of a diagram with the AUC plotted versus the duration of the time-window of cumulated precipitation considered in the ROC (Fig. 4b). By means of this plot, assuming that an AUC above 0.7 indicates an acceptable discriminant, it is possible to assess which minimal time window must be considered, for each specific prism, in order to obtain a ROC curve with an AUC of 0.7 (hereafter referred to as time window of "first significance") and which time window must be considered in order to reach a maximum AUC (hereafter referred to as time window of "maximum significance").
- Retrieval, from each ROC curve associated to the considered time windows, of the values of precipitation associated to the Max. Dist. and Max. TSI points and of the Max. TP-precipitation value.
- Generation, on the basis of data from the previous step, of prism-specific Max. Dist. curve, Max. TSI curve and Max. TP-precipitation curve to be displayed in a precipitation (mm) versus precipitation moving window (days) plot.
- Generation, by averaging values from all prisms, of mean Max. Dist. curve, Max. TSI curve and Max. TP-precipitation curve in the precipitation (mm) versus precipitation moving window (days) plot (Fig. 4c). In practice, the Max. TSI curve represents a more conservative threshold in comparison to the Max Dist. curve since, by definition, the TSI minimizes also the occurrence of false alarms. Moreover, the Max. TP-precipitation curve envelopes all maximum precipitation values corresponding to a TP event in the dataset. Thus, the area above it represents extreme precipitation conditions that, in the monitoring period, have never been exceeded when a TP event occurred.

- Test and validation of the predictive performances of Max. Dist. curve and Max. TSI curve. This is performed by computing the TP-rate and FP-rate of $V_{95\%}$, prediction in the validation dataset with respect to 10, 20 and 40 days cumulated precipitation (identified as the most effective cumulative intervals) and by assessing the results in the ROC space.
- Subdivision of the cumulative precipitation (mm) vs. precipitation moving windows (days) plot into four potential warning levels of the exceedance of $V_{95\%}$ thresholds, on the basis of Max. Dist., Max. TSI and Max. TP-precipitation curves.
- Simulation of how precipitations recorded in two past episodes of acceleration of the whole Piagneto landslide would be characterised in terms of warning levels (see discussion section). This is performed by displaying the precipitation records of these periods in the cumulative precipitation (mm) vs. precipitation moving windows (days) plot.

Results

The ROC curves obtained for the monitoring prisms evidence that the AUC tend to increase at increasing duration of the cumulative window duration. However, above a given duration of the cumulative window, the AUC tends to decrease (see, as an example, the ROC curves of figure 4d, which refer to prism n.3). Consequently, when the AUC of the various ROC curves obtained with all the prisms is plotted against the cumulative window duration, the trend is generally bell shaped (Fig. 5). The maximum AUC is, for many prisms, higher than 0.9, a value that is associated to models with excellent discriminant capacity. The time-window of first significance (i.e. the time window at which AUC > 0.7) lies around 10 days in prisms from all the different rock slide units and in the debris slide. The time-window of maximum significance (i.e. time window at which AUC = max) is generally reached at around 40 days. The AUC remains above 0.7 up until around 70 days or more. Therefore, time windows of cumulated precipitation ranging from 10 to 70 days are in this case study appropriate to discriminate the behaviour of the landslide in terms of velocity, with best predictive capacity with 40 days cumulated precipitation. However, some prisms located in the middle unit of the landslide, show an AUC trend that keeps increasing at increasing time window duration. In these cases, the time window of "first significance" is shifted toward higher values and the time window of "maximum significance" is practically unreached.
The resulting Max. Dist. curve, Max. TSI curve and Max. TP-precipitation curve (which have been obtained by averaging all the ROC curves associated to each prism at all the considered time windows), are presented in figure 6. These curves show that the mean cumulated precipitation to be reached in order to exceed $V_{95\%}$ is respectively 71 mm/10 days, 148 mm/20 days and 311 mm/40 days in the Max. Dist. Curve and 133 mm/10 days, 219 mm/20 days and 396 mm/40 days in the Max. TSI Curve. The predictive performance of prism-specific Max. Dist. and Max. TSI curves picked at 10, 20 and 40 days cumulative time windows has been verified by using the validation dataset and the ROC approach. In both cases, the maximum TP-rate equals to 1 in several prisms and FP-rates are always lower than 0.4 (Fig. 7). Results related to Max TSI curves provide better performances as they provide minimum FP-rates. With both Max TSI and Max. Dist., the distribution of TP-rates and FP-rates is correlated to the duration of the precipitation cumulative window. Better performances are generally achieved for the 40 days cumulated precipitation period, while performances tend to decrease when considering the 20 and 10 days cumulated precipitation. It should be noticed that the TP-rate to FP-rate ratio is significantly higher, at 20 and 40 days cumulated windows, for prisms in the front landslide units, indicating a better predictive capacity of the adopted method for the front units.

Discussion

In comparison to other methods proposed in literature for forecasting the velocity of landslides based on precipitation data (selected references are provided in the introduction section) the proposed approach has different advantages, disadvantages and limits of applicability. One of the main advantages is that it directly returns the duration and quantity of precipitation that discriminates the occurrence of a given value of landslide velocity. This can be used to analyse slope processes and, possibly, to support the assessment of early warning rules. Another asset, which is common to nonlinear and statistical models, is that it is evidence based, since it relies exclusively on displacement and precipitation monitoring data. Thus, it does not require any data of underground geometries and geotechnical and hydrogeological parameters, that are indeed quite difficult to be properly assessed in large landslides and that are necessary for the application of physical and numerical simulation approaches. On the other hand, one of the drawback is that it can only be applied to landslides that show recurrent changes in velocity in response to precipitation and that have been monitored for quite long periods of time, since the input dataset must contain a sufficiently large number of events on the basis of which discriminant relationships can be obtained. This limits the possibility to replicate the proposed approach, as many phenomena might not show such type of temporal movement pattern or might not have been monitored with sufficient temporal resolution or duration. This limitation that does not apply for nonlinear, physical and numerical simulation models that, however,

also generally require quite long time series of monitoring data in order to be properly calibrated. Moreover, similarly to nonlinear and statistical models, the proposed approach can only be used to discriminate the precipitation conditions leading to the occurrence of high velocity events in the range of these monitored in the past. Thus, it cannot be used to directly predict paroxysmal events that have not yet occurred in the period of monitoring. This prediction is instead generally possible with physical and numerical simulation models, but its reliability depends significantly upon the critical assumption that the model remains valid also for displacements rates that might be out of the range used in model calibration.

Nevertheless, the exceedance of "rare" velocity values in a monitoring dataset can be considered as a warning signal for a possible significant and risky evolution of the landslide. In practical terms, the Max. Dist., Max. TSI and Max. TP-precipitation curves generated in this research allow to subdivide the cumulated precipitation (mm) – precipitation moving window (days) plot into four zones that indicate increasing probability of exceeding $V_{95\%}$ velocities. Consequently, these zones can possibly be associated to different warning levels (e.g. W1 – ordinary; W2 – attention; W3 – alert; W4 – alarm, as in figure 8). To verify the operational applicability of these thresholds, precipitation records related to two different "critical" periods at the Piagneto landslide have been plotted in the diagram: (i) the January 2014 event (inside the monitoring period, during which, on the 22nd of Jan., more than the 50% of the monitoring prisms suddenly recorded velocities higher than $V_{95\%}$, after being below such threshold for several previous months); (ii) the September 1972 event (outside the monitoring period, when a few days after the 11th of Sept. the collapse of blocks triggering a debris slide which buried National Road SS63, see case study section). The simulation referring to January 2014 (Fig. 9), shows that 30 days before the critical period the ongoing precipitation curve is entirely in the W1 zone. However, already 21 days before the event, the precipitation curve enters the W2 zone at short cumulated time windows. Gradually, 7 days before the critical period, it reaches the W3 zone at short cumulated time windows and the W2 zone at the 20-40 days window (that are characterised by the best statistical significance based on the AUC). This shows that the obtained results could have been profitably used for warning, with almost a week advance, about the upcoming critical period. On the other hand, with respect to the simulation of September 1972 period (characterized by a 300 mm precipitation on the 11th of Sept.), the precipitation thresholds enter the W2 zone on 9th Sept. and the W4 zone on 11th Sept. (see Fig. 10). Since the exact day of the landslide collapsed and debris slide is unreported, it is not actually possible to estimate to how many days of effective early warning our method should have given. Nevertheless, the simulation clearly indicates that paroxysmal events can be correctly indicated by ongoing precipitation curves that would lay above the W4 alarm threshold.

Conclusions

The research has allowed to develop and test an approach for the use of ROC curves in the discriminant analysis of the relationships between cumulated precipitation and movement rates in active landslides and to verify its potential applicability for early warning purposes. The approach is based on displacement and precipitation monitoring data and allows the duration and the quantity of precipitation that discriminates the occurrence of landslide velocities or acceleration values exceeding certain thresholds to be determined. The approach has been successfully tested in a complex landslide characterized by recurrent variations of velocity in response to precipitation and by variable movement rates in different parts of the landslide, as proven by a 5-year long dataset of daily movements collected by using an RTS measuring 20 prisms located in the slope. The velocity thresholds used in the test site have been normalized by using the $V_{95\%}$ values calculated for each monitoring prism, i.e. rare values that during the 5 years of monitoring were exceeded in only 5% of the days. Based on the results, one main finding is that time-windows from 10 to 40 days are appropriate to discriminate the occurrence of $V_{95\%}$ values based on cumulated precipitation in the test site and that the threshold curves obtained with the proposed method are capable of supporting early warning for the exceedance of high, and possibly critical, velocity values. The adopted approach is replicable in any case study with recurrent changes of velocity in response to precipitation and the achieved results proved their efficiency for the definition of early warning levels based on cumulated precipitation.

Acknowledgements

This work was supported by the Civil Protection Agency of the Emilia-Romagna Region under the framework agreement "Special activities on support to the forecast and emergency planning of Civil Protection with respect to hydrogeological risk" (ASPER-RER, 2011–2015). The authors wish to acknowledge Francesco Bonacini, Giuseppe Caputo, Francesco Ronchetti and Giovanni Truffelli for their collaboration of in the setup and management of the RTS monitoring systems and field surveys and Marcello Petitta for some exchange of opinions on the applied methodology. The authors wish to thank Jordi Corominas (UPC, Spain) for suggesting the use of ROC curves in the analysis of the Piagneto landslide dataset.

References

Abellán A, Michoud C, Jaboyedoff M, Baillifard F, Demierre J, Carrea D, Derron MH (2015) Velocity Prediction on Time-Variant Landslides Using Moving Response Functions: Application to La Barmasse Rockslide (Valais, Switzerland), in: Lollino G, Giordan D, Crosta GB, Corominas J, Azzam R, Wasowski J, Sciarra N (eds) Engineering Geology for Society and Territory - Volume 2 SE - 49. Springer International Publishing, pp 323–327. doi:10.1007/978-3-319-09057-3_49

Belle P, Aunay B, Bernardie S, Grandjean G, Ladouche B, Mazué R, Join JL (2014) The application of an innovative inverse model for understanding and predicting landslide movements (Salazie cirque landslides, Reunion Island). Landslides 11:343–355. doi:10.1007/s10346-013-0393-5

Bernardie S, Desramaut N, Malet JP, Gourlay M, Grandjean G (2014) Prediction of changes in landslide rates induced by rainfall. Landslides 12:481-494. doi:10.1007/s10346-014-0495-8

Bernardie S, Desramaut N, Malet JP, Azib M, Grandjean G (2015) Prediction of the Rainfall-Induced Landslides: Applications of FLAME in the French Alps. in: Lollino G, Giordan D, Crosta GB, Corominas J, Azzam R, Wasowski J, Sciarra N (eds) Engineering Geology for Society and Territory - Volume 2 SE - 49. Springer International Publishing, pp 647-651. doi: 10.1007/978-3-319-09057-3_108

Bracegirdle A, Vaughan PR, Hight DW (1991) Displacement prediction using rate effects on residual strength. In: Bell DH (ed), Landslides, Proceedings of the VIth International Symposium on landslides, Christchurge. Balkema, Rotterdam, pp 343–347

Butterfield R (2000) A dynamic model of shallow slope motion driven by fluctuating ground water level, In: Bromhead E, Dixon N, Ibsen ML (eds) Landslides in Research, Theory and Practice. Thomas Telford Ltd, pp 203-208

Chung CJF and Fabbri AG (2003) Validation of Spatial Prediction Models for Landslide Hazard Mapping. Nat Hazards 30:451– 472. doi:10.1023/B:NHAZ.0000007172.62651.2b

Corominas J, Moya J, Ledesma A, Lloret A, Gili JA (2005) Prediction of ground displacements and velocities from groundwater level changes at the Vallcebre landslide (Eastern Pyrenees, Spain). Landslides 2:83–96. doi:10.1007/s10346-005-0049-1

Corsini A, Castagnetti C, Bertacchini E, Rivola R, Ronchetti F, Capra A (2013a) Integrating airborne and multi-temporal long-range terrestrial laser scanning with total station measurements for mapping and monitoring a compound slow moving rock slide. Earth Surf Proc Land 38:1330–1338. doi:10.1002/esp.3445

Corsini A, Ronchetti F, Bertacchini E, Bonacini F, Calicetti P, Capra A, Castagnetti C, Piantelli E, Caputo G, Truffelli G. (2013b) Large-scale slope instability affecting SS63 near the Cerreto Pass (northern Apennines, Italy). In Margottini C, Canuti P, Sassa K (eds) Landslide Science and Practice. Volume 6: Risk Assessment, Management and Mitigation, Springer, Berlin Heidelberg, pp. 231–237. doi:10.1007/978-3-642-31319-6_32

Corsini A, Mulas M, Petitta M, Bonacini F, Ronchetti F, Caputo G, Truffelli G (2015a) Prediction of landslide velocity at given cumulated rainfall values based on analysis of continuous monitoring data using ROC curves: application to the Piagneto landslide (Northern Apennine, Italy). EGU General Assembly 2015. Geophysical Research Abstracts Vol. 17, EGU2015-7264-1

Corsini A, Bonacini, F, Mulas M, Petitta M, Ronchetti F, Truffelli G (2015b) Long-Term Continuous Monitoring of a Deep-Seated Compound Rock Slide in the Northern Apennines (Italy), in: Lollino G, Giordan D, Crosta GB, Corominas J, Azzam R, Wasowski J, Sciarra N (eds) Engineering Geology for Society and Territory - Volume 2 SE - 49. Springer International Publishing, pp 1337–1340. doi:10.1007/978-3-319-09057-3_235

Donner RV and Barbosa SM (2008) Nonlinear Time Series Analysis in the Geosciences: Applications in Climatology, Geodynamics and Solar-Terrestrial Physics. Springer, Berlin Heidelberg

Herrera G, Fernandez-Merodo JA, Mulas J, Pastor M, Luzi G, Monserrat O (2009) A landslide forecasting model using ground based SAR data: The Portalet case study. Eng Geol 105:220–230. doi:10.1016/j.enggeo.2009.02.009

Iverson RM (2000) Landslide triggering by rain infiltration. Water Resour Res 36:1897-1910. doi:10.1029/2000WR900090

Hosmer DW and Lemeshow S (2000) Applied Logistic Regression. 3rd ed. John Wiley & Sons, Inc

Leroueil S. (2000) Contribution to the round table: Peculiar aspects of structured soils. in Evangelista A and Picarelli L (eds) The geotechnics of hard soils – soft rocks: Proceedings of the second International Symposium on Hard Soils – Soft Rocks, Naples, Italy, 12-14 October 1998 Volume 3. Rotterdam, the Netherlands: A. A. Balkema. 3:1669-1677

Li X, Kong J, Wang Z (2012) Landslide displacement prediction based on combining method with optimal weight. Nat. Hazards 61:635–646. doi:10.1007/s11069-011-0051-y

Li X, Kong J (2014) Application of GA–SVM method with parameter optimization for landslide development prediction. Nat Hazards Earth Syst Sci 14:525–533

Liu Z, Shao J, Xu W, Chen H, Shi C (2014) Comparison on landslide nonlinear displacement analysis and prediction with computational intelligence approaches. Landslides 11:889–896. doi:10.1007/s10346-013-0443-z

Lollino G, Arattano M, Allasia P, Giordan D (2006) Time response of a landslide to meteorological events. Nat Hazard Earth Sci 6:179–184. doi:10.5194/nhess-6-179-2006

Mayoraza F and Vulliet L (2002) Neural networks for slope movement prediction. Int J Geomech 2:153–173. doi:10.1061/(ASCE)1532-3641(2002)2:2(153)

Moratti L and Pellegrini M (1977) Alluvioni e dissesti verificatisi nel 1972 e 1973 nei bacini dei fiumi Secchia e Panaro (Province di Modena e Reggio Emilia). Bollettino della Associazione Mineraria Sudalpina, Torino, anno XIV, n. 2, giugno 1977. 323-374

Nordvik T and Nyrnes E (2009) Statistical analysis of surface displacements – an example from the Aknes rockslide, western Norway. Nat. Hazards Earth Syst. Sci., 9:713–724. doi:10.5194/nhess-9-713-2009

R Development Core Team (2008) R: A language and environment for statistical computing. R Foundation for Statistical Computing. Vienna, Austria. ISBN 3-900051-07-0, URL http://www.R-project.org

Ronchetti F, Borgatti L, Cervi F, Lucente CC, Veneziano M, Corsini A (2007) The Valoria landslide reactivation in 2005–2006 (Northern Apennines, Italy). Landslides 4:189–195. doi:10.1007/s10346-006-0073-9

Schädler W, Borgatti L, Corsini A, Meier J, Ronchetti F, Schanz T (2015) Geomechanical assessment of the Corvara earthflow through numerical modelling and inverse analysis. Landslides, 12:495–510. doi:10.1007/s10346-014-0498-5

Swets JA (1988) Measuring the accuracy of diagnostic systems. Science 240(4857):1285-1293. doi:10.1126/science.3287615

Zhang WJ, Chen YM, Zhan LT (2006) Loading/Unloading response ratio theory applied in predicting deep-seated landslides triggering. Eng. Geol. 82:234–240. doi:10.1016/j.enggeo.2005.11.005

Vulliet L and Hutter K (1988) Viscous-type sliding laws for landslides, Can Geotech J, 25:467–477

Figure captions

Fig. 1 (a) Location of the Piagneto landslide. (b) Geological setting and geomorphic zonation of the landslide. (c) Frontal view of the G2 sub-unit.

Fig. 2 (a) Dataset: cumulative displacements and daily precipitation (grey) recorded at the Piagneto landslide. (b) Position of the monitoring prisms and localization of units of the G2 sector. (c) Recorded average annual velocities. (c) $V_{95\%}$ velocity of each prism referred to the Training dataset.

Fig. 3 Approach for the application of ROC curves to the Piagneto landslide monitoring dataset. (a) Example of the classification problem statement: given a precipitation threshold (blue line) and a velocity threshold (red line) all the given records are classified into TP, FN, FP and TN. (b) General formulation for TP-rate, FP-rate, TSI and applied conditions for classification of events. (c) Construction of ROC curve with respect to a given velocity threshold with cumulated precipitation in a given number of antecedent days as the variable parameter ranging from zero precipitations value to the maximum recorded by that cumulative window.

Fig. 4 Exemplification of the procedure used for the analysis of ROC curves. (a) Plot of ROC curves obtained for each monitoring prism (nominally prisms I, II, III) with respect to different time-windows of cumulated precipitation (for example 1 = 10 days, 2 = 45 days, 3 = 90 days): the Area Under Curve (AUC) and the maximum distance from the line of no discrimination are calculated. (b) Analysis of the variation of the AUC for the prisms I, II, III with respect to different time-windows of cumulated precipitation: in detail prism III (green line) denotes an anomalous trend with the AUC continuing increasing with larger time window. (c) Precipitation threshold curves necessary to exceed $V_{95\%}$ velocities dividing the plot area into four "Warning Zones" (W1 to W4). (d) ROC curves obtained for the $V_{95\%}$ velocity threshold of the monitoring prism *G2_03* with respect to different precipitation moving window.

Fig. 5 Variation of Area Under the ROC Curve (AUC) for the different monitoring prisms with respect to different precipitation moving window considering $V_{95\%}$ thresholds.

Fig. 6 Precipitation threshold curves necessary to exceed $V_{95\%}$ identified using the training dataset. Each point of the Max Dist. and Max TSI curves is referred to a given cumulative time window and mean value of the precipitation thresholds of all prisms are obtained. Max. TP-precipitation curve identifies the maximum precipitation value occurred for each cumulative window when a TP event has been identified.

Fig 7 Performances of precipitation thresholds identified after the training phase in terms of FP-rate and TP-rate represented according to the landslide unit in which each prism is located: 1) Rear; 2) Middle; 3) Front; 4) Debris slide. (a) Performances of thresholds derived using the Max TSI criterion; (b) Performances of thresholds derived using the Max Distance criterion.

Fig. 8 (a) Representation of the ROC derived precipitation thresholds for early warning: the "Warning Zones" are depicted together with the statistical significance of precipitation moving windows.

Fig. 9 (a) Daily precipitations from Dec. 2013 to Jan. 2014; (b) to (g) Representation of the occurring precipitation curve (black dashed line) from 30 days before the 22/01/2014 critical period, with respect to the precipitation threshold curves.

Fig. 10 (a) Daily precipitations from August to September 1972; (b) to (g) Representation of the occurring precipitation curve (black dashed line) from 30 days before the 11/09/1972 critical period, with respect to the precipitation threshold curves.

Figure 1

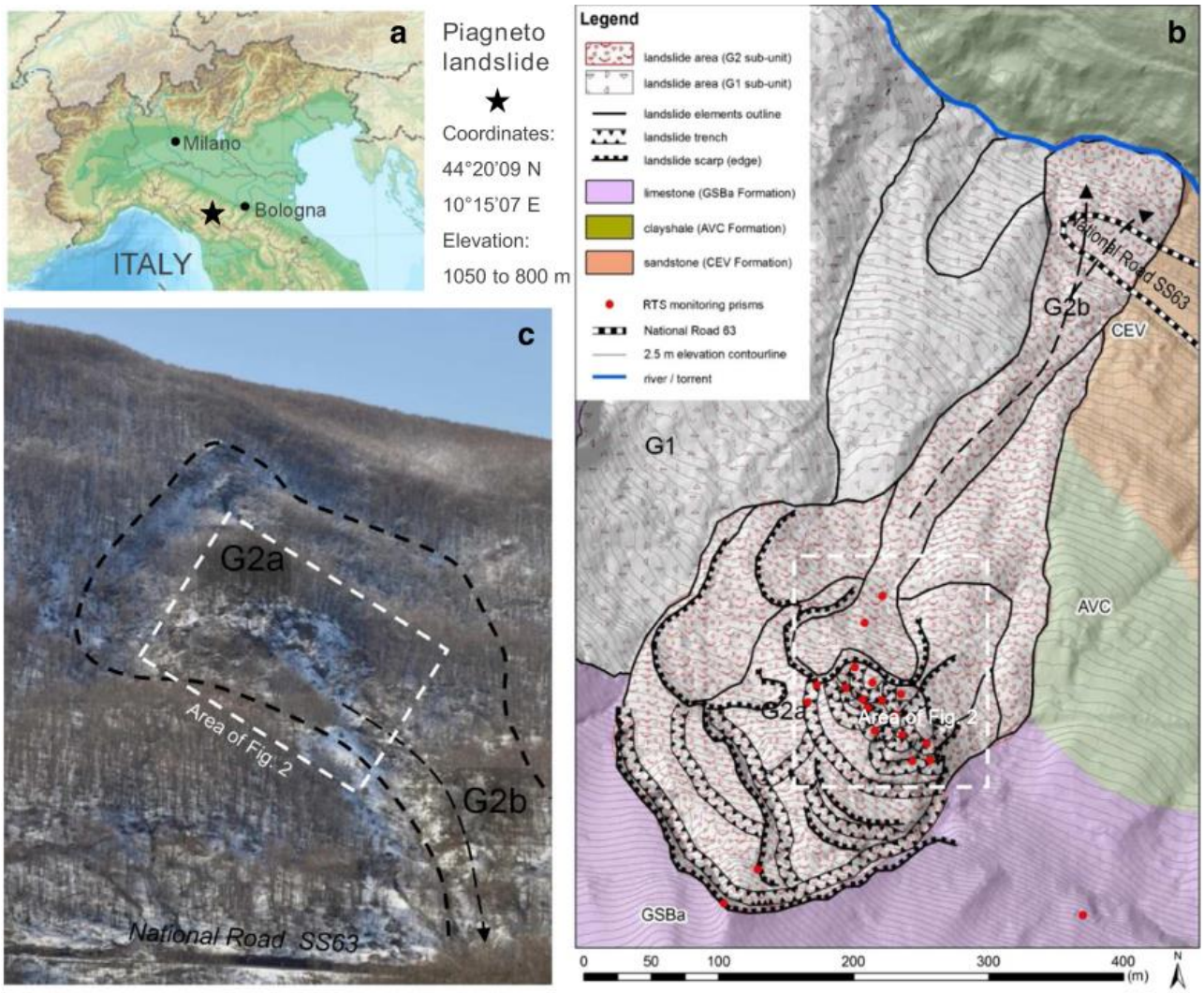
a
Milano
Bologna
ITALY
Piagneto landslide
Coordinates:
44°20'09 N
10°15'07 E
Elevation:
1050 to 800 m
b
Legend
landslide area (G2 sub-unit)
landslide area (G1 sub-unit)
landslide elements outline
landslide trench
landslide scarp (edge)
limestone (GSBa Formation)
clayshale (AVC Formation)
sandstone (CEV Formation)
RTS monitoring prisms
National Road 63
2.5 m elevation contourline
river / torrent
G1
G2a
G2b
CEV
AVC
GSBa
National Road SS63
Area of Fig. 2
0
50
100
200
300
400
(m)
N
c
G2a
G2b
Area of Fig. 2
National Road SS63

Figure 2

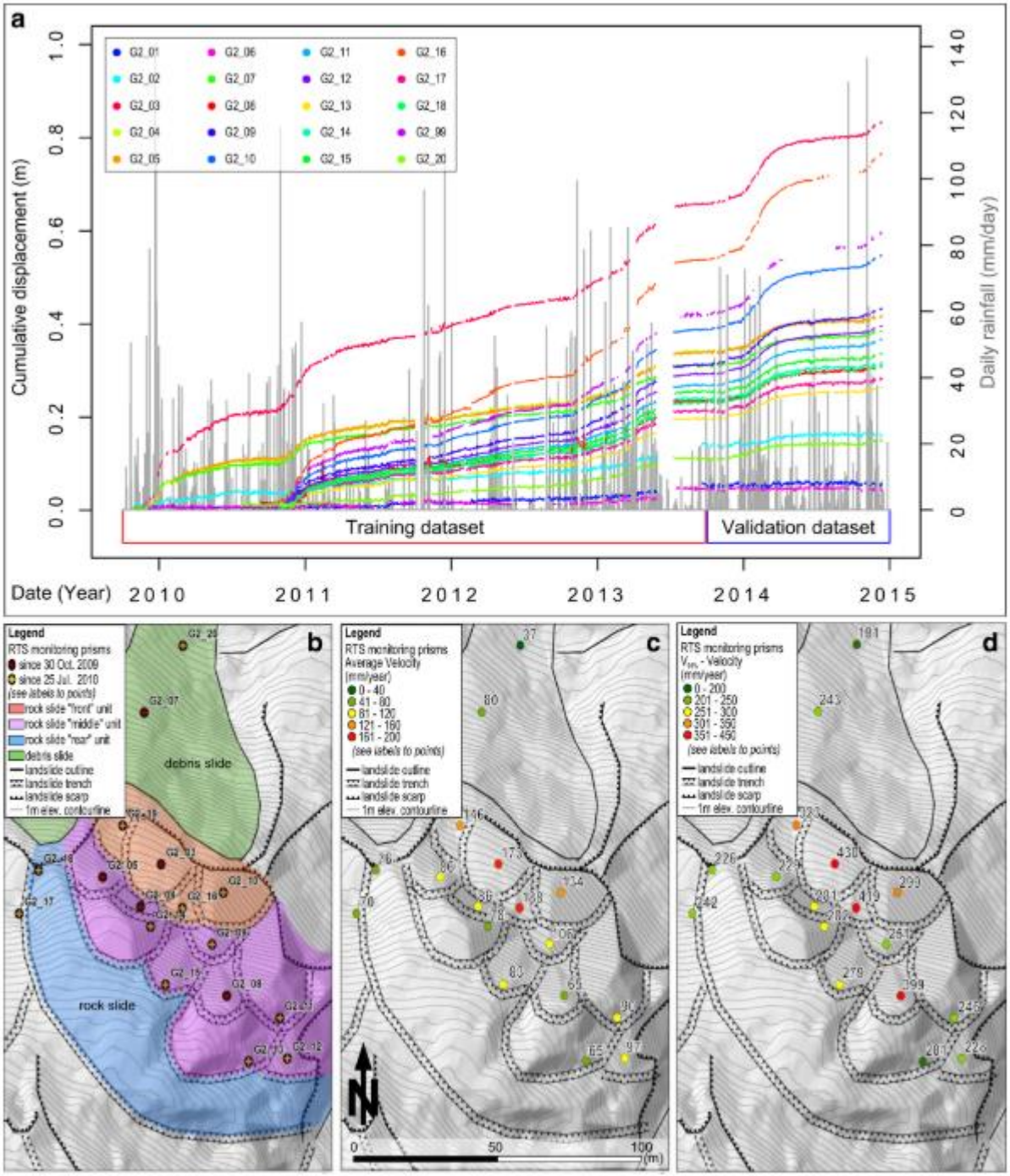
a
Cumulative displacement (m)
Daily rainfall (mm/day)
Training dataset
Validation dataset
Date (Year)
2010
2011
2012
2013
2014
2015
b
debris slide
rock slide
c
d
0
50
100
(m)

Figure 3

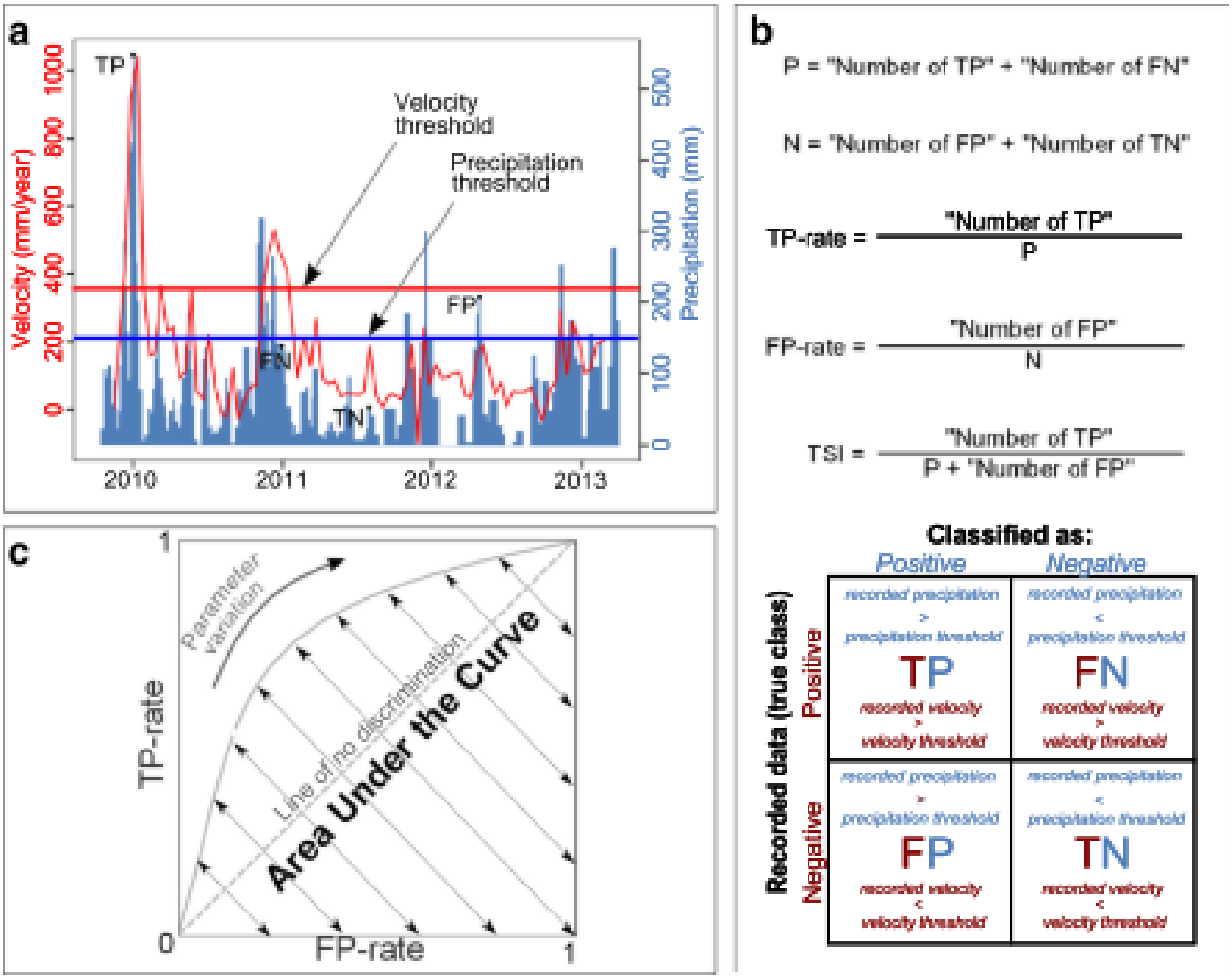
a
TP
Velocity threshold
Precipitation threshold
FP
FN
TN
Velocity (mm/year)
Precipitation (mm)
2010
2011
2012
2013
b
P = "Number of TP" + "Number of FN"
N = "Number of FP" + "Number of TN"
TP-rate = "Number of TP" / P
FP-rate = "Number of FP" / N
TSI = "Number of TP" / P + "Number of FP"
Classified as:
Positive
Negative
Recorded data (true class)
recorded precipitation > precipitation threshold
recorded precipitation < precipitation threshold
TP
FN
recorded velocity > velocity threshold
recorded velocity < velocity threshold
FP
TN
c
Parameter variation
Line of no discrimination
Area Under the Curve
TP-rate
FP-rate
0
1

Figure 4

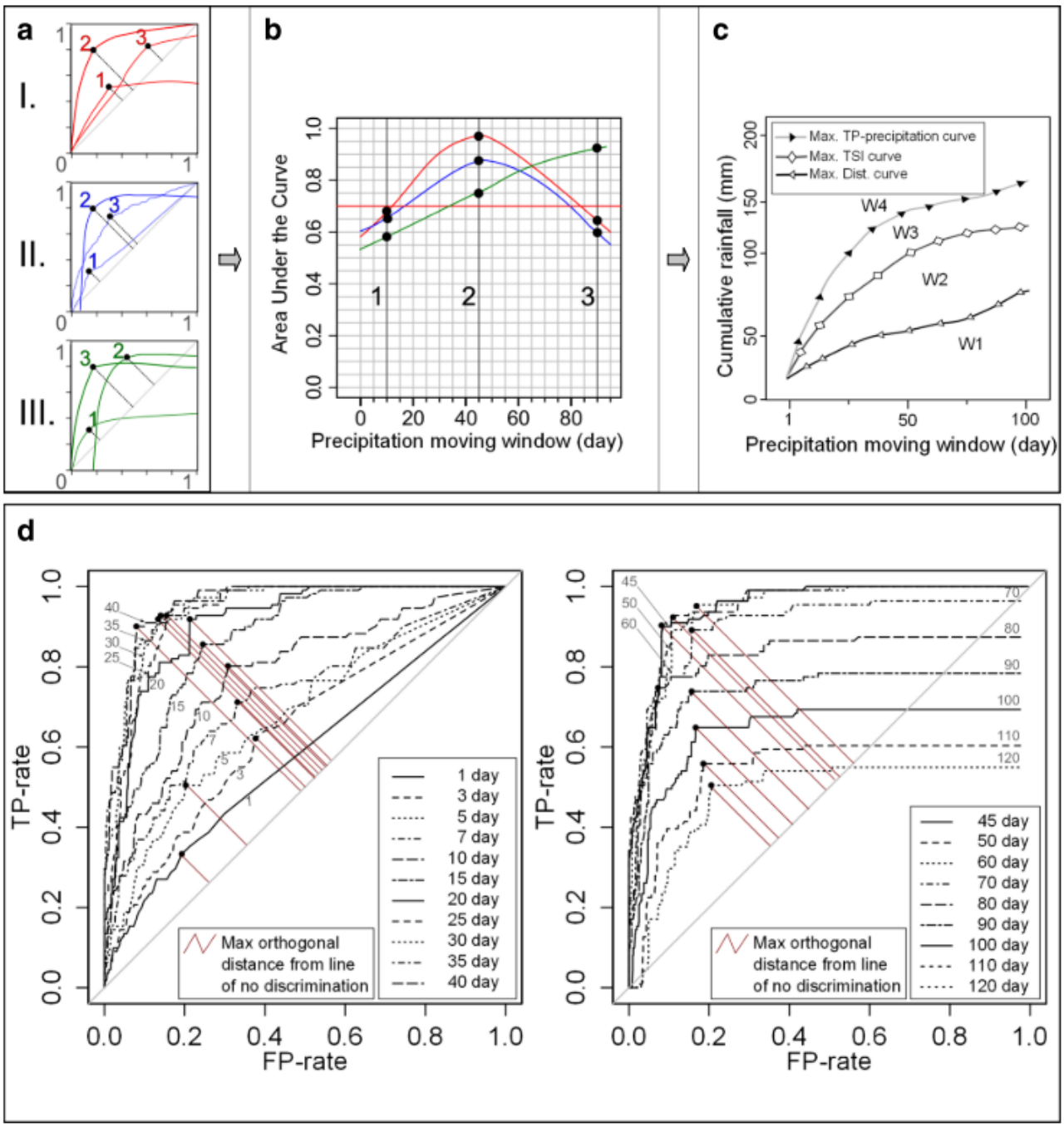
a
I.
II.
III.
b
Area Under the Curve
Precipitation moving window (day)
c
Max. TP-precipitation curve
Max. TSI curve
Max. Dist. curve
Cumulative rainfall (mm)
W4
W3
W2
W1
Precipitation moving window (day)
d
TP-rate
FP-rate
Max orthogonal distance from line of no discrimination
1 day
3 day
5 day
7 day
10 day
15 day
20 day
25 day
30 day
35 day
40 day
45 day
50 day
60 day
70 day
80 day
90 day
100 day
110 day
120 day

Figure 5

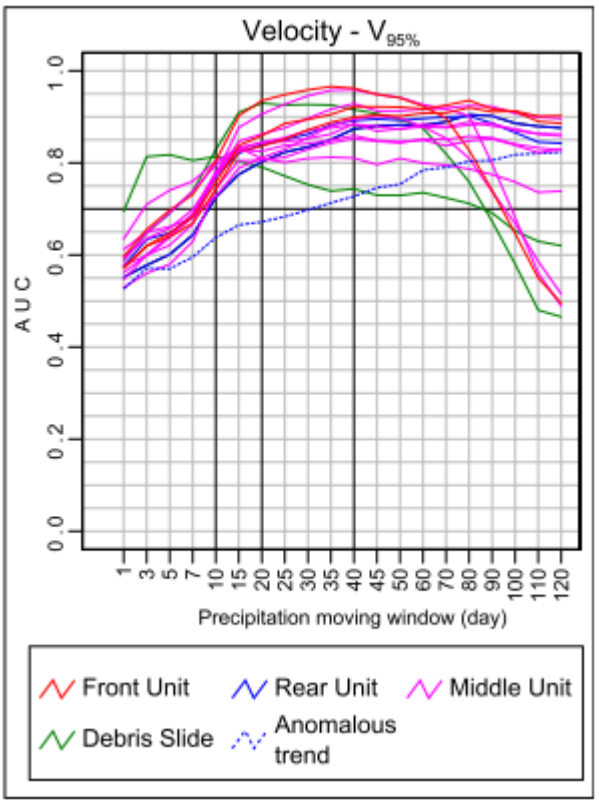

Figure 6

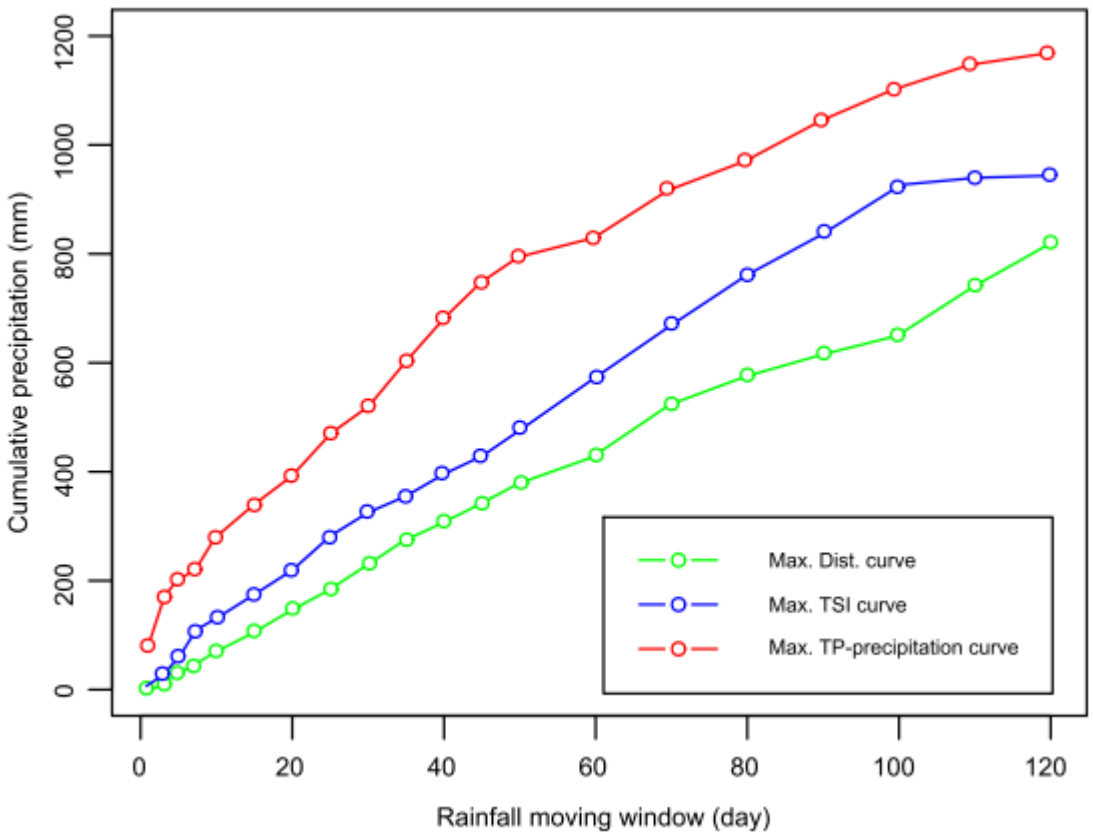

Figure 7

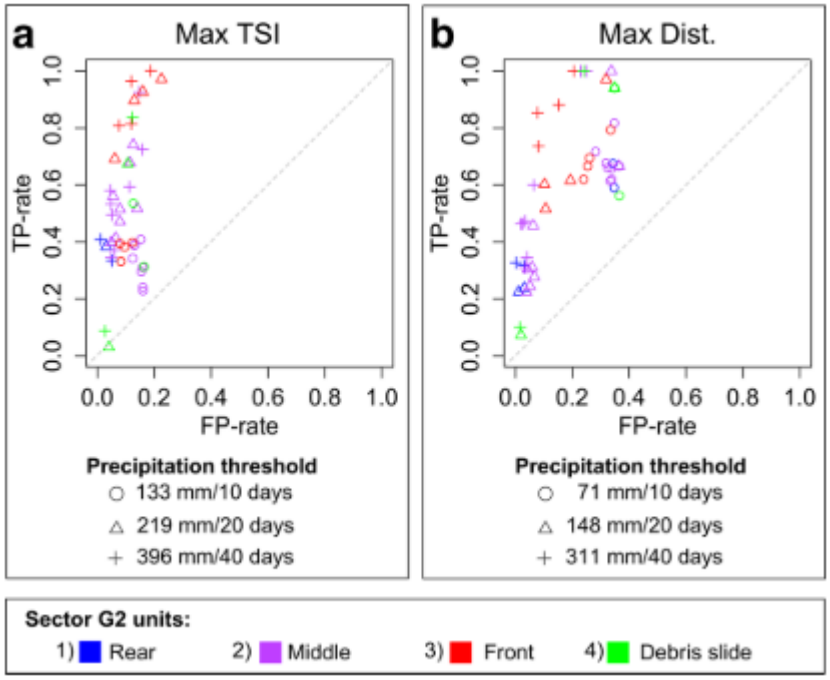

Figure 8

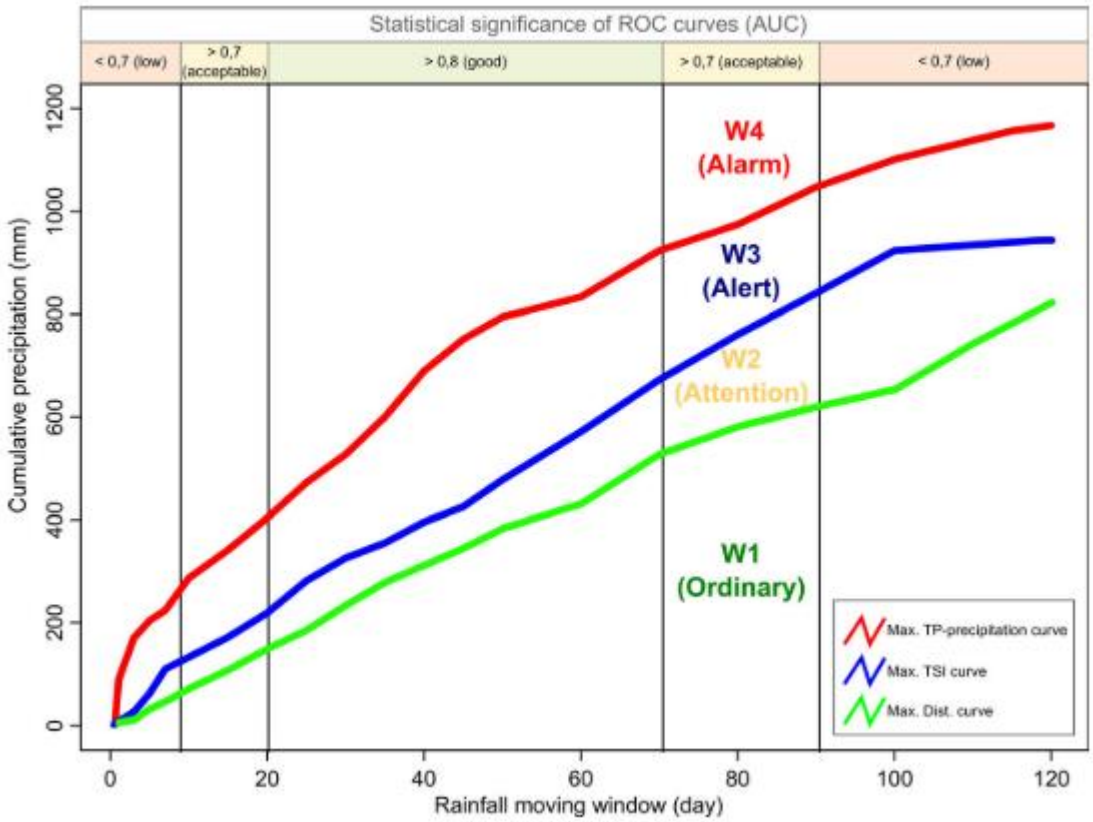

Figure 9

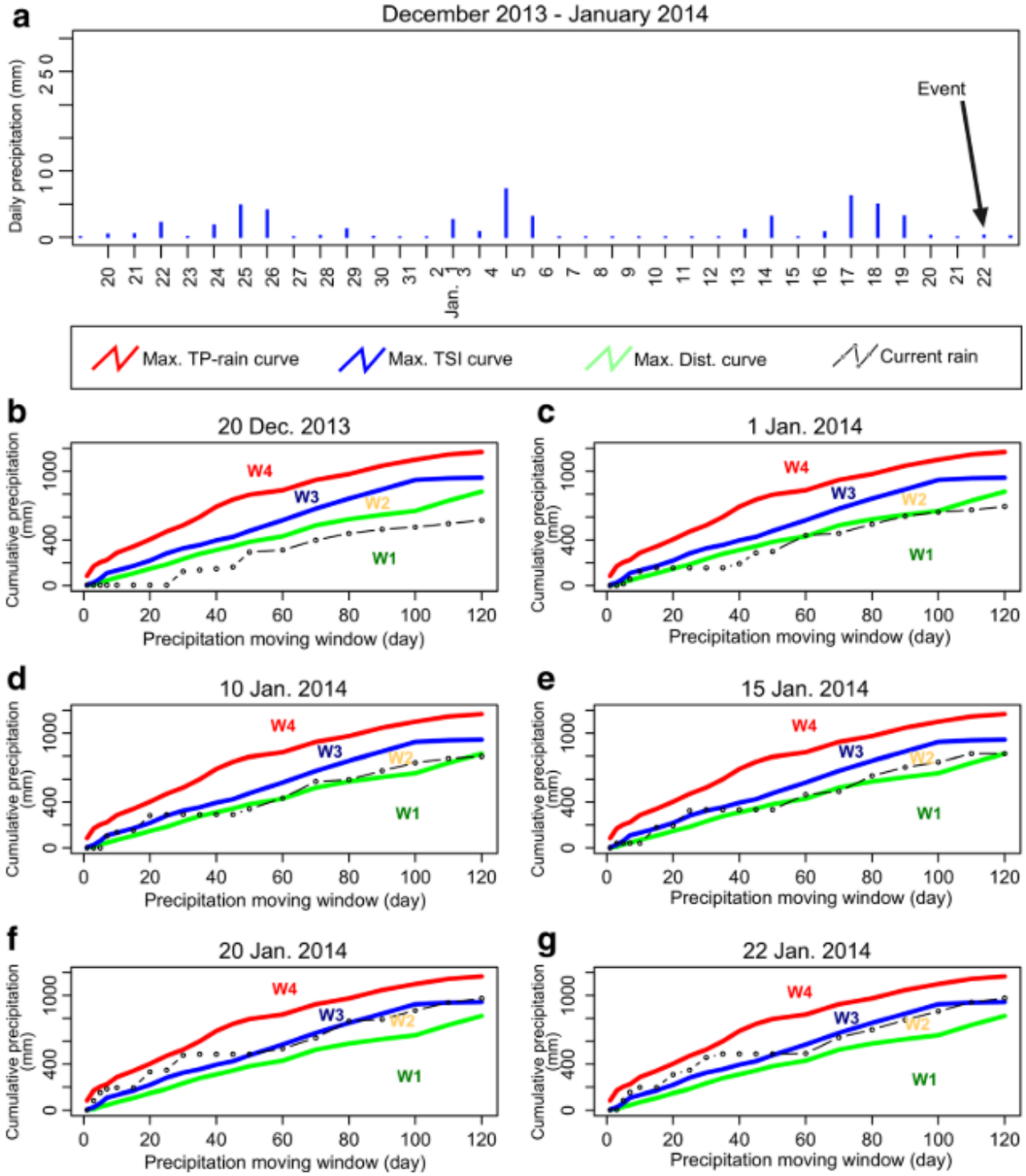
a
December 2013 - January 2014
Daily precipitation (mm)
Event
Jan.
Max. TP-rain curve
Max. TSI curve
Max. Dist. curve
Current rain
b
20 Dec. 2013
c
1 Jan. 2014
d
10 Jan. 2014
e
15 Jan. 2014
f
20 Jan. 2014
g
22 Jan. 2014
Cumulative precipitation (mm)
Precipitation moving window (day)
W4
W3
W2
W1

Figure 10

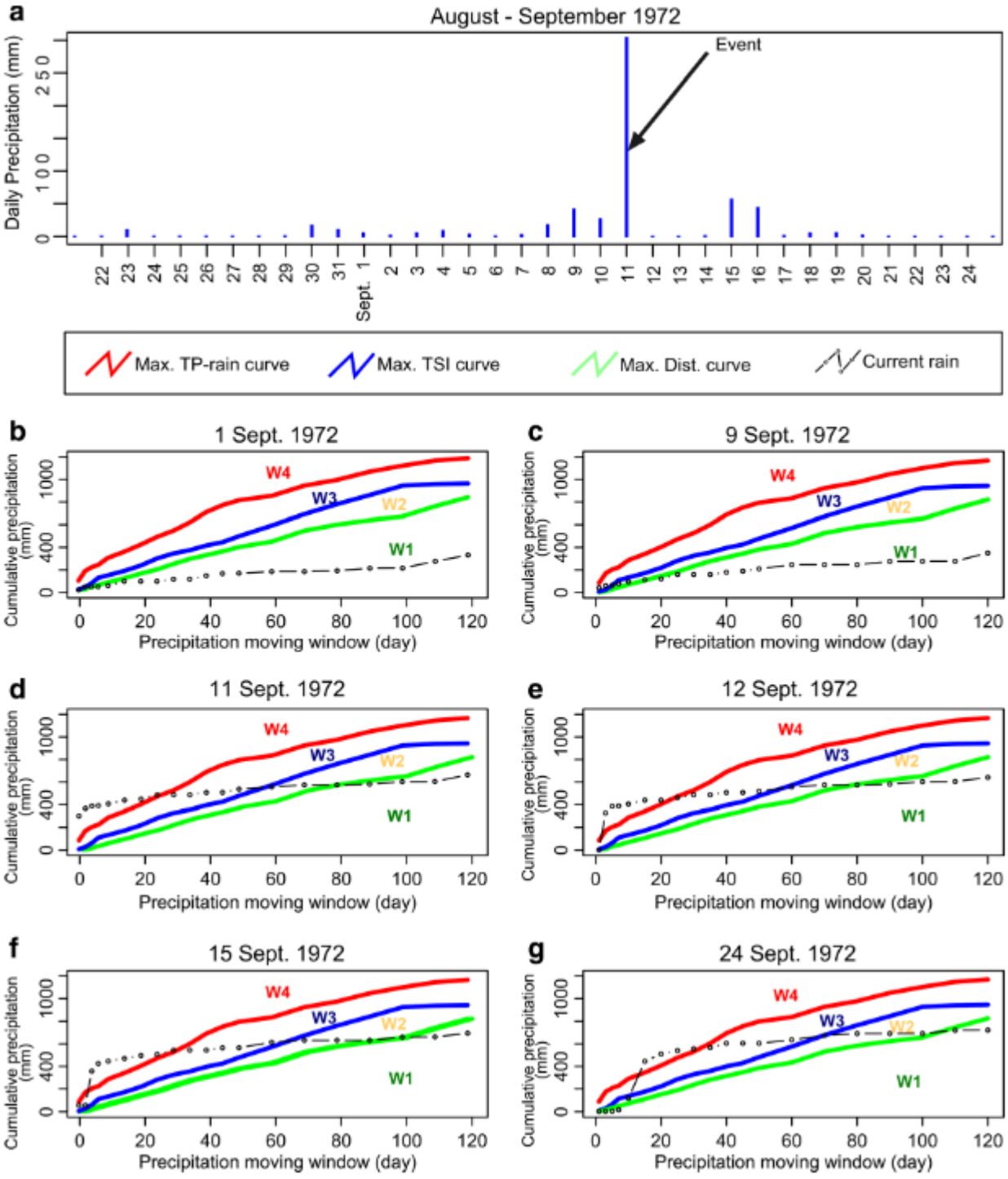
a
August - September 1972
Daily Precipitation (mm)
Event
Sept.
Max. TP-rain curve
Max. TSI curve
Max. Dist. curve
Current rain
b
1 Sept. 1972
c
9 Sept. 1972
d
11 Sept. 1972
e
12 Sept. 1972
f
15 Sept. 1972
g
24 Sept. 1972
W4
W3
W2
W1
Cumulative precipitation (mm)
Precipitation moving window (day)